

# Substrate effects on surface magnetism of Fe/W(110) from first principles

Torsten Andersen<sup>1</sup> and Wolfgang Hübner<sup>1</sup>

<sup>1</sup>Department of Physics, Kaiserslautern University of Technology, Box 3049, D-67653 Kaiserslautern, Germany

(Dated: March 23, 2022; Revised)

Surface magnetic properties of the pseudomorphic Fe(110) monolayer on a W(110) substrate are investigated from first principles as a function of the substrate thickness (up to 8 layers). Analyzing the magnetocrystalline anisotropy energies, we find stable (with respect to the number of substrate layers) in-plane easy and hard axes of magnetization along the  $[1\bar{1}0]$ - and  $[001]$ -directions, respectively, reaching a value in good agreement with experiment for thick substrates. Additionally, the changes to the magnetic spin moments and the density of the Fe  $d$ -states are analyzed with respect to the number of substrate layers as well as with respect to the direction of magnetization. With respect to the number of W(110) substrate layers beneath the Fe(110) surface, we find that the first four substrate layers have a large influence on the electronic and magnetic properties of the surface. Beyond the 4th layer, the substrate has only marginal influence on the surface properties.

PACS numbers: 75.70.Ak, 75.70.Rf, 73.20.At

## I. INTRODUCTION

The pseudomorphic monolayer of Fe grown on a W(110) surface is very interesting from the point of view of magnetism. In studies of the surface magneto-crystalline anisotropy, the Fe monolayer on top of a W substrate has become the system of choice, since (i) the growth of the first Fe monolayer is pseudomorphic, (ii) the W substrate has a large spin-orbit coupling, and (iii) the interface anisotropy is the strongest ever observed. This makes the Fe monolayer on a W substrate a good candidate for an *ab initio* benchmark investigation of how the properties of the magneto-crystalline anisotropy are influenced by the substrate.

Depending on the coverage and the surface orientation, Fe films on a W substrate show very different magnetic properties. At submonolayer coverages on the (110) surface one observes the formation of separate islands that are nonmagnetic up to a coverage of 58-60%, beyond which they become ferromagnetic islands,<sup>1</sup> which may even show an out-of-plane magnetization until they approach the full-monolayer coverage.<sup>2</sup> A single monolayer (ML) of Fe can be grown pseudomorphically on top of a W(110) surface.<sup>3</sup> Experiments performed on the pseudomorphic Fe monolayer<sup>4,5,6,7,8,9</sup> have shown that<sup>5</sup> “the prominent magnetic feature of Fe(110) films on W(110) is a strong in-plane magnetic surface anisotropy, with an easy axis  $[110]$  at right angles to the bulk easy axis  $[001]$ .” At coverages of about 1.5 ML, double-layer patches (sesquilayers) form with an out-of-plane magnetic easy axis,<sup>10</sup> and an antiferromagnetic order.<sup>11,12</sup> A pseudomorphic full second ML has to our knowledge not been grown experimentally, but theory predicts it would also have an in-plane easy axis in the  $1\bar{1}0$ -direction.<sup>13</sup> Attempts of using annealing as a means of making the grown Fe layers full monolayers beyond the first monolayer leads to a reorganization of the Fe in an Fe bulk-like lattice.<sup>14</sup> For continuous layers of Fe, the easy axis of magnetization eventually changes to the in-plane  $[001]$ -direction it has in bulk Fe,<sup>15,16,17,18</sup> the critical thickness of the Fe film being reported in the range between 80 and 95 Å (95 Å reported by Ref. 16, and 80–86 Å reported by Ref. 18).

In passing, we should stress that in contrast to the ferro-

magnetic Fe monolayer on the W(110) surface stand results of recent studies (experimental<sup>19,20</sup> and *ab initio*)<sup>20,21,22</sup> of Fe films on the (001) surface of W, which indicate that the first ML of Fe is antiferromagnetic when grown on the (001) surface. Thus, the magnetic properties of the Fe monolayer is very sensitive to the surface orientation of the W substrate, and one can not make general conclusions about the magnetic properties of other surfaces on the basis of investigations of only one.

In the present work, we study the substrate effects on the magnetic properties of the pseudomorphic ML of Fe(110) on W(110) from first principles. Existing *ab initio* calculations performed within the full-potential linearized augmented plane-wave (FLAPW) method,<sup>13,23,24</sup> the full-potential linearized muffin-tin orbital (FP-LMTO) method,<sup>25</sup> as well as pseudo-potential calculations<sup>21</sup> confirm the above-mentioned experimental ferromagnetic result with an easy axis along the  $[1\bar{1}0]$ -direction. At present, there is no measurable lattice-relaxation effect of the magnetization direction,<sup>26</sup> and the starting point for the calculations presented in this work is the optimized surface of Ref. 23. The main results of our work are magnetocrystalline anisotropy energies that are converged *ab initio* as a function of the substrate thickness, along with magnetic spin- and orbital moments that consistently confirm the breaking of Hund’s 3rd rule for the W substrate. The quality of the results is illustrated by explicitly showing the convergence, along with an estimate of the accuracy.

The paper is organized as follows: in Sec. II we describe and discuss the method that we use, in particular with respect to the level of accuracy necessary for the calculation of stable magnetocrystalline anisotropy energies, and in Sec. III we present and discuss the results of our calculations, where we focus the attention on the magnetic and electronic properties of the surface, and how the substrate influences these properties. Finally, in Sec. IV, we conclude.

## II. METHOD

Since we have the flexibility that a theoretical calculation provides, we do not need to limit ourselves to the experimen-

tally possible. Thus, we are able to take an approach where we begin with a bilayer of Fe(110) and W(110), successively adding W substrate layers underneath in order to investigate how the sub-surface layers influences the magnetic and electronic properties at the surface.

In order to facilitate the calculation of magnetocrystalline anisotropy energies and how they change with the number of substrate layers, one has to perform the calculations with a highly accurate and mature *ab initio* computer code. The demands on accuracy imply that a full-potential code is necessary. Since all *ab initio* methods employs an “educated guess” for the initial solution, the code *must* be self-consistently reaching a stable solution to the eigenvalue problem of the Schrödinger equation, e.g., by use of the Rayleigh-Ritz<sup>27,28</sup> variational approach. In addition to this, the spin-orbit interaction must be included in the self-consistent solution in order to produce magnetic properties that are accurate enough. The *ab initio* method of choice for our calculations is the full-potential (partially linearized) augmented plane-wave [(L)APW+lo] with local orbitals method<sup>29</sup> as implemented in the WIEN2K computer code.<sup>30</sup>

Within the WIEN2K code, one constructs a supercell perpendicular to the surface, ensuring that enough vacuum is inserted between the surface and the border of the unit cell (in our case the vacuum amounts to at least 16 interlayer distances of the W(110) substrate). In order to keep the environment of our surface calculation stable, we let the Fe monolayer sit in the middle of the unit cell of constant size, adding the W substrate layers under it. This choice, of course, limits our possibility for continuously adding W substrate layers, but not beyond the practical limits of the code, as we shall see later.

In a study where we begin from the surface layer we expect to see rather big changes to the electronic and magnetic properties as we add substrate layers to the system, due to the similarities to the properties of a quantum well. As we keep adding substrate layers we expect the properties to stabilize in such a manner that the system starts behaving like a surface layer on a bulk-like substrate. When this point has been reached, adding another substrate layer should not change the electronic and magnetic properties at the Fe surface layer much.

With our demands on the accuracy, it is important that the surface is structurally relaxed. How a single monolayer of Fe(110) relaxes on top of a W(110) substrate has been studied by Qian and Hübner (Ref. 23). Since their results are very close to experiment,<sup>1,4,5,6,7,8,11,31</sup> and since there is no experimentally measurable structural effect due to changes in the direction of magnetization,<sup>26</sup> we have in the present work chosen to adopt the optimized surface structure of Ref. 23 as the basis for our calculations. We have, however, in order to better describe the influence of the substrate on the surface magnetism, chosen to use a nonsymmetric layered structure instead of the symmetric one of Ref. 23. Thus, the structure is using the optimized values of the interlayer distances from the surface side as determined in Ref. 23 [the Fe-W1 distance is contracted by 12.9% and the W1-W2 distance by 0.1% compared to bulk W(110) interlayer distances (W1 and W2 are the first and second W layers under the Fe layer, respectively)], but has bulk-spaced W layers underneath. The Fe layer has

an in-plane lattice misfit of about 10% compared to a pure Fe(110) surface.

In practical *ab initio* calculations within density-functional theory, one has to make a choice of the so-called exchange-correlation potential, since it is not known as an exact quantity. Our calculations within the WIEN2K computer code are performed using the [generalized gradient approximation (GGA)] exchange-correlation potential of Perdew, Burke, and Ernzerhof (Ref. 32). In order to facilitate the calculation of magnetic anisotropy energies (MAEs), the variational parameter, i.e., the total energy of the *magnetic* configuration,<sup>33</sup> was converged to an accuracy that in most cases is better than 10  $\mu$ Ry (for a detailed list of relevant accuracies, consult the results section, in particular Tab. I). Also, the fluctuations in the charge density within the unit cell has been converged to less than  $10^{-4}$  e/Bohr<sup>3</sup>. Since the abovementioned two convergence criteria do not automatically ensure that the eigenstates and eigenfunctions are sufficiently accurate, one has in addition to make sure that also the calculation converges with respect to the parameters that control the accuracy of the calculations of the WIEN2K code [in particular the (kinetic energy) cutoff value of the otherwise infinite plane-wave basis, and the sampling in  $\mathbf{k}$ -space]. As we shall illustrate below, these parameters were adjusted (increased) until the magnetic anisotropy energies for an increasing number of W layers stabilized.

The parameter used to control the kinetic energy cutoff of the plane-wave basis depends on the muffin-tin radius used for the atomic part of the (L)APW basis set as follows:

$$T_c = R_{\text{MT}} k_{\text{max}}, \quad (1)$$

where  $T_c$  is the cutoff parameter,  $R_{\text{MT}}$  is the muffin-tin radius (2.35 Bohr in our calculations), and  $k_{\text{max}}^2$  corresponds to the plane-wave cutoff (in Ry) in pseudopotential calculations, e.g., the value  $T_c = 9$  gives a  $k_{\text{max}}^2 = 199.56$  eV. Thus,  $T_c$  determines the matrix size of the eigenvalue problem, and higher values of  $T_c$  potentially decreases the accuracy of the resulting eigenfunctions and -energies.

### III. RESULTS AND DISCUSSION

When one begins with an Fe/W(110) bilayer and thereafter add W(110) substrate layers (on the W side of the bilayer), one expects that as long as the number of W layers (called  $N_W$  in the following) is sufficiently small, the system behaves in a quantum-well-like fashion, i.e., the changes to properties such as the magnetocrystalline anisotropy energy or the density of states will be large each time a substrate layer is added. At some critical value of  $N_W$ , one would expect that the substrate starts behaving like a bulk substrate and, thus, that the Fe layer becomes more surface-like in its properties. Below, we discuss how the magnetocrystalline anisotropy energies and the electronic structure change as a function of  $N_W$ .

TABLE I: (Color online) Evolution of the magnetocrystalline anisotropy energy of the Fe/W(110) surface as a function of (i) the number of W layers beneath the pseudomorphic Fe monolayer included in the calculation,  $N_W$ , (ii) the kinetic energy cutoff of the plane-wave basis,  $T_c = R_{MT} k_{\max}^2$  [below,  $T_c = 7$  corresponds to  $k_{\max}^2 = 120.72$  eV,  $T_c = 8$  to  $k_{\max}^2 = 157.68$  eV, and  $T_c = 9$  to  $k_{\max}^2 = 199.56$  eV], and (iii) the number of  $\mathbf{k}$ -points in the full Brillouin zone,  $\#\mathbf{k}$ . The leftmost half of the table shows how the total energy of the surface magnetized along the easy axis,  $\mathbf{M}||[1\bar{1}0]$  evolve as a function of  $T_c$ ,  $\#\mathbf{k}$ , and  $N_W$ . The first column is the number of W layers, the second column is the total energy at  $\{T_c, \#\mathbf{k}\} = \{7, 441\}$ , columns 2–6 show the evolution of this total energy as the accuracy of the calculation increases (as the difference in total energy with respect to the previous calculation), and in column 7 is shown the total energy of the converged calculation along with the uncertainty estimate, as given by Eq. (2). In columns 8–12 is shown how the MAE of the perpendicular magnetization direction ( $\mathbf{M}||[110]$ ) changes during convergence, where in column 12 the uncertainty estimate has been added. Column 13 lists the converged MAEs for  $\mathbf{M}||[001]$  with their respective uncertainty estimates (for the uncertainties of  $\mathbf{M}||[001]$  relative to  $\mathbf{M}||[110]$ , see the text). Each and every number in this table have been determined self-consistently.

$N_W$	Total energy for $\mathbf{M}  [1\bar{1}0]$						MAE with respect to $\mathbf{M}  [1\bar{1}0]$ (meV)					
	(MeV)	evolution (meV)				Final (meV)	$\mathbf{M}  [110]$					$\mathbf{M}  [001]$
	$T_c$ :	7	8	8	9	9	7	8	8	9	9	9
	$\#\mathbf{k}$ :	441	441	961	961	2025	441	441	961	961	2025	2025
1	-0.474538	-574	0.75	-157	0.18	<b>-474539186.379±0.034</b>	0.80	-0.03	-0.80	0.29	<b>0.11±0.08</b>	<b>1.77±0.12</b>
2	-0.914445	-917	0.46	-257	0.11	<b>-914445985.433±0.068</b>	4.53	4.61	3.81	4.63	<b>4.75±0.10</b>	<b>6.00±0.11</b>
3	-1.354351	-1257	-0.44	-354	0.53	<b>-1354352832.665±0.034</b>	2.57	2.79	2.12	3.29	<b>3.16±0.16</b>	<b>3.66±0.11</b>
4	-1.794257	-1595	-1.13	-448	-0.33	<b>-1794259724.579±0.061</b>	2.45	3.29	2.76	2.68	<b>2.34±0.15</b>	<b>2.82±0.19</b>
5	-2.234164	-1931	-0.07	-546	-0.73	<b>-2234166567.988±0.041</b>	3.61	2.34	0.11	1.97	<b>2.08±0.15</b>	<b>2.57±0.21</b>
6	-2.674070	-2263	-3.20	-638	-0.41	<b>-2674073400.852±0.054</b>	2.04	2.03	0.98	1.97	<b>2.60±0.18</b>	<b>2.79±0.14</b>
7	-3.113976	-2592	-1.85	-738	-0.80	<b>-3113980210.383±0.136</b>	2.80	1.67	0.19	2.07	<b>2.72±0.31</b>	<b>3.01±0.38</b>
8	-3.553883	-2921	-5.07	-823	0.24	<b>-3553887008.444±0.258</b>	3.70	2.27	-0.03	2.29	<b>2.26±0.53</b>	<b>2.99±0.41</b>

### A. Magnetocrystalline anisotropy energies

Searching for magnetocrystalline anisotropy energies on the basis of *ab initio* methods that minimizes the total energy, one is looking for energy differences in the meV-range which has to be calculated from differences between total energies in the MeV-range. In order to provide us with two significant digits in the meV-range it is required that the computed total energies are numerically accurate to (within the limits of the physical model) the 11th decimal. Today's standard arithmetic precision (64-bit numbers with a 52-bit mantissa) provides 16 significant digits, and thus already a sum over 1000  $\mathbf{k}$ -points reduces precision to 13 significant digits at best. Carefully written self-consistent full-potential methods may limit the further loss of precision caused by sampling, but the amount of  $\mathbf{k}$ -points is limited if one wants to obtain meaningful results.

In order to be able to draw any conclusions about the substrate effects and the properties of the surface for a fixed geometry, the calculation of the MAEs must first converge with respect to, in particular, the kinetic energy cutoff of the plane-wave basis, as well as the sampling in  $\mathbf{k}$ -space.<sup>34</sup> Since MAEs are calculated here as differences of “total energies”, this requirement automatically applies to the “total energies” (even though the “total energies” are not necessarily physically meaningful quantities themselves). Thus, the evolution of the magnetocrystalline anisotropy energies of the Fe/W(110) surface is described in Tab. I as a function of (i) the number of W layers added underneath the pseudomorphic Fe monolayer, (ii) the kinetic energy cutoff of the plane-wave basis, as defined by Eq. 1, and (iii) the number of sampling points ( $\mathbf{k}$ -points) used in the full Brillouin zone (FBZ), here called  $\#\mathbf{k}$  in a short notation. In order to make the numbers

directly comparable and to avoid pure  $\mathbf{k}$ -point effects, calculations on the same level of accuracy have been performed with the *same*  $\mathbf{k}$ -points (in the FBZ), and the volume of the “unit cell” has been kept constant. Since MAEs are differences in “total energies”, Tab. I consists of two main blocks, namely (left) the evolution of the total energy of the ground state, which is the system that is magnetized along the *easy* magnetic axis, here  $\mathbf{M}||[1\bar{1}0]$  in agreement with experiment (see Refs. 1,4,5,6,7,8,11,31,35) and theory (see Ref. 23); and (right) the evolution in the MAEs with respect to the easy axis for the out-of-plane direction,  $\mathbf{M}||[110]$ . The rightmost column shows the converged MAEs for the in-plane direction that is perpendicular to the easy axis, i.e., the *hard* axis  $\mathbf{M}||[001]$ .

The far left column lists the number of W layers added underneath the pseudomorphic Fe surface layer. Columns 2–7 show results for the total energy of the systems with magnetization along the easy axis. Column 2 shows the total energy in MeV of the cheapest calculation (lowest value of  $T_c$  and lowest number of  $\mathbf{k}$ -points) performed in this study. Column 3 shows the difference in the total energy (with respect to the results in column 2) when one increases the kinetic energy cutoff. One observes that the total energy increases with about 340 meV per W atom. In column 4, the density of the sampling in  $\mathbf{k}$ -space is increased, with changes in the total energy compared to the results in column 3 of less than a meV per atom. Increasing  $T_c$  again in column 5, the total energy changes at most 100 meV per W atom, and the calculation has become so stable that a further increase in the sampling in  $\mathbf{k}$ -space (column 6) gives rise to changes in the total energy of less than 1 meV. Increasing  $T_c$  beyond the value of 9 introduces ghost bands, and self-consistent minimization of the total energy is not possible. With the small changes in the to-

tal energy occurring in column 6, however, together with the stability seen in the MAEs in the right half of the table, leads us to conclude that the calculation has converged with respect to  $T_c$  and  $\#k$ . Thus, in column 7 we have listed the total energies in meV for the calculation from column 6 to the  $\mu\text{eV}$ -level, together with an estimate of the uncertainty obtained in the self-consistent minimization procedure. This uncertainty is calculated from the total energies of the last three cycles of the self-consistent minimization of the total energy. Let  $n$  refer to the last cycle, then the uncertainty  $\varepsilon(n)$  on the total energy  $V(n)$  in the last cycle is calculated as:

$$\varepsilon(n) = [|V(n) - V(n-1)| + |V(n) - V(n-2)|] / 2. \quad (2)$$

The smallest uncertainty achieved in the present calculation is 2.5  $\mu\text{Ry}$  (34  $\mu\text{eV}$ ). We notice in passing that at 7 and 8 substrate layers, the uncertainties become larger. Beyond 8 substrate layers, the calculations become less stable, i.e., the required level of accuracy in order to calculate well converged MAEs could not be reached.

In the right half of Tab. I are listed the MAEs that come out, when the calculations in columns 2–7 are repeated for  $\mathbf{M}||[110]$  and the results for the easy-axis calculation are subtracted. Hence, since all “total energies” are negative, positive numbers indicate that the absolute value of the total energy is smaller than that of the easy-axis calculation, and thus we can conclude that the axis is “harder”. Similarly, negative values indicate that the axis is “easier”, and one notices immediately that in the two right-most calculations (columns 11 and 12) there are no negative values (for  $T_c = 9$ ). Column 13 lists the MAEs for  $\mathbf{M}||[001]$ . Here we have left out the evolution, since it shows behaviour similar to the MAEs for  $\mathbf{M}||[110]$ . It is important to underscore the fact that each of the numbers that appear in Tab. I is a result of an individual self-consistent minimization of the total energy and the fluctuations in the charge density for the specific configuration. In Tab. I, three columns are in red. The numbers in these columns are the final, converged, results, and are listed with their individual level of uncertainty. Naturally, the uncertainties of the total energy for the easy axis are small compared to those of the MAEs. The uncertainties listed for the MAEs are calculated as the sums of the uncertainties for the total energies of the two calculations involved in getting a single MAE. One should bear in mind that the uncertainties between the results for  $\mathbf{M}||[110]$  and  $\mathbf{M}||[001]$  are *not* simply an addition of the uncertainties listed in columns 12 and 13 of Tab. I, since the uncertainties listed are on the MAEs, *not* the total energy, and thus with respect to  $\mathbf{M}||[1\bar{1}0]$ . The relative uncertainties between the results for  $\mathbf{M}||[110]$  and  $\mathbf{M}||[001]$  are (in meV):  $\pm 0.20$  for 1 W layer,  $\pm 0.07$  for 2 W layers,  $\pm 0.20$  for 3 W layers,  $\pm 0.31$  for 4 W layers,  $\pm 0.19$  for 5 W layers,  $\pm 0.16$  for 6 W layers,  $\pm 0.39$  for 7 W layers, and  $\pm 0.37$  for 8 W layers. With these values in mind, it is safe to conclude that the magnetic *hard* axis is in the  $[001]$ -direction.

In order to visualize the influence of the substrate on the magnetocrystalline anisotropy energies, we have in Fig. 1 plotted the MAEs relative to the easy axis ( $\mathbf{M}||[1\bar{1}0]$ ) with respect to the number of W layers in the substrate under the Fe(110) monolayer, along with their respective uncertainties

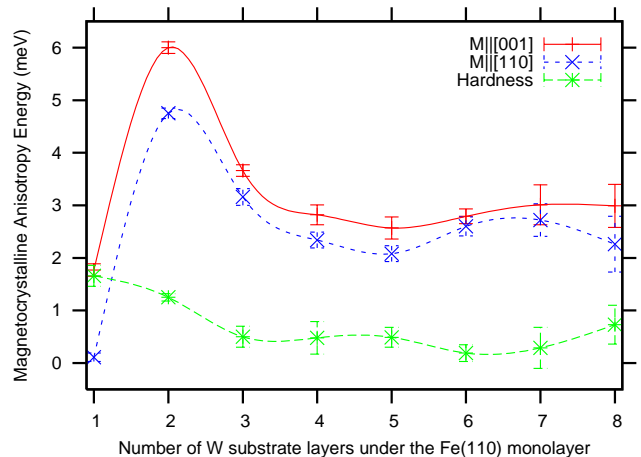


FIG. 1: (Color online) Magnetic anisotropy energies relative to the easy axis ( $\mathbf{M}||[1\bar{1}0]$ ) are shown as a function of the number of W substrate layers underneath the Fe(110) surface layer. Data are taken from Tab. I and the text, and the uncertainties have been included as vertical error bars in the plot. The red (full line) and blue (short-dashed line) curves show the MAEs of the  $[001]$ - and  $[110]$ -directions, respectively. The green (long-dashed line) curve shows the energy difference between samples magnetized along the  $[001]$  and  $[110]$  directions, which also can be called the degree of hardness of the hard axis (see text). To guide the eye, cubic splines have been used to connect the data points.

(indicated by a vertical bar at each data point). In order to guide the eye, cubic splines have been included to connect the data points. The red (upper) line shows the evolution of the MAE of the in-plane hard  $[001]$  axis, while the blue line shows how the MAE of the direction perpendicular to the surface  $[110]$  evolves when adding substrate layers. The green (bottom) line shows the MAE between the hard and the perpendicular axes, and can thus be interpreted as the “hardness” of the hard axis. As long as it is positive, the hard axis is along the in-plane  $[001]$ -direction, whereas if it became negative the hard axis would shift to being out-of-plane.

The trend in the values of the MAEs is clear. At one layer of W, the MAEs are small, but at two layers of W one sees a dramatic increase, and the MAEs reaches their maximum values. Adding a 3rd layer of W, the MAEs drop again, and from the 4th layer and on they get almost constant, in agreement with Ref. 25. The value at the “bulk” end (7–8 substrate layers) is, with its 3 meV quite close to the experimental value of 4.2 meV obtained recently by Pratzer, Elmers, *et al.* (Ref. 35) for Fe monolayer stripes on W(110). That the values differ by about 1 meV could have its origin in the fact that the experiment is made on stripes. Since the stripes have lower symmetry than a perfect monolayer we would expect the MAE to be slightly higher for the stripes. Older experiments<sup>12,17,36,37</sup> give values of the MAEs in the range from about 0.11 meV to about 6.5 meV, depending on the setup, temperature, and film thickness.

Table I and Fig. 1 reveal a magnetic hard axis along the  $[001]$ -direction. That the absolute values<sup>38</sup> differ from those of Ref. 13 can be attributed to the fact that we are using asym-

TABLE II: Magnetic anisotropy energies for different magnetization directions in 1 ML of Fe on top of 4 ML of W(110). The anisotropy energies are with respect to the value of the total energy for  $\mathbf{M} \parallel [1\bar{1}0]$ . Here,  $T_c = 9$  and  $\#\mathbf{k}=2025$ , and the uncertainties are calculated as in Tab. I by use of Eq. (2). The first four rows are in-plane and the last four rows out-of-plane (see text).

Magnetization direction	MAE (meV)
5° from $[110]$ towards $[001]$	$0.15 \pm 0.09$
$[1\bar{1}1]$	$0.83 \pm 0.17$
5° from $[001]$ towards $[1\bar{1}0]$	$2.82 \pm 0.09$
$[001]$	$2.82 \pm 0.19$
5° from $[001]$ towards $[110]$	$2.53 \pm 0.22$
5° from $[1\bar{1}0]$ towards $[110]$	$2.31 \pm 0.21$
5° from $[1\bar{1}1]$ towards $[110]$	$2.59 \pm 0.20$
$[110]$	$2.34 \pm 0.15$

metric structures (with an Fe layer only on one side of the slab) in the present work, whereas Ref. 13 used symmetric structures (with an Fe layer on both sides of the slab).

### B. Magnetic properties of the electronic structure

In order to verify that the easy axis is really along one of the main crystallographic axes (and along the  $[1\bar{1}0]$ -direction) we have performed a number of calculations of the total energy where the magnetization direction has been shifted by 5° away from the main crystallographic axes (in various directions, as indicated in Tab. II). These calculations have been performed for four substrate layers only. Thus, we have in Tab. II printed the MAEs with respect to the magnetic easy axis for  $T_c = 9$  and  $\#\mathbf{k} = 2025$ . In Tab. II, the first four lines show the development of the MAE as we change the magnetization from the easy axis to the hard axis in the surface plane, the next three lines show how the MAE changes as we go away from the surface, and the last line shows the value perpendicular to the surface. The values along the hard and perpendicular axes are taken from Tab. I. It is important to stress that in order for the results in Tab. II to be trustworthy (since the MAEs are calculated from total energies), one needs to make the calculations identical in the sense that *only* the direction of magnetization is allowed to change. The critical quantity to keep identical here is the  $\mathbf{k}$ -space sampling-mesh (total energies are  $\mathbf{k}$ -dependent, as is evident from Tab. I). The results in Tab. II are therefore all obtained with the exact same  $\mathbf{k}$ -points (in the Full Brillouin Zone), regardless of the changes in symmetry.

Of the first four lines in Tab. II, the first line shows the result when the magnetization direction is shifted by 5° in the direction of the hard axis. When the magnetization is shifted further in the direction of the hard axis, one passes the crystallographic  $[1\bar{1}1]$ -direction (second line of Tab. II) that could be a natural place to look for an easy or hard axis of magnetization. As we can see, it is neither the easy- nor the hard axis. Close to the hard axis (c), the anisotropy at 5° away from it has a value that is very close to (equal to, in fact, within our precision) that of the hard axis. The value for the hard axis MAE is shown for reference in the fourth line. Going 5° out of the sur-

face from the three axes  $[1\bar{1}0]$ ,  $[1\bar{1}1]$ , and  $[001]$ , we again see values between those of the easy and hard axes. In fact, the change in the MAE by going 5° out of the surface plane from the easy axis is quite strong. Thus, we conclude from Tab. II that evidence is strong enough for to confirm that the easy axis is along the (in-plane)  $[1\bar{1}0]$ -direction, in agreement with previous experimental<sup>1,4,5,6,7,8,11,31</sup> and theoretical<sup>13,25</sup> findings.

Tab. III lists the magnetic spin- ( $\mu_S$ ) and orbital ( $\mu_L$ ) moments per atom for the three different magnetization directions we consider. First, we notice in general that the magnetic spin moment of the Fe atom is enhanced in comparison to the bulk fcc Fe value of 2.2  $\mu_B$ . Second, in all three cases, after peaking at about 2.61  $\mu_B$  for 3 substrate layers, the Fe atom takes on a magnetic spin moment of about 2.56  $\mu_B$ , and the first W layer under the Fe surface layer takes on a moment of about 0.1  $\mu_B$  in the opposite direction (hence, it is antiferromagnetically coupled to the Fe layer), consistent with the result of Ref. 39. The remaining magnetic spin moments, including the interstitial moments, are negligible (less than 1.5% of the Fe moment).

Looking at the orbital moments in Tab. III ( $\mu_L$ ), we observe that while the spin moments do not change their sign with a change of the magnetization axis, the orbital moments do. With magnetization along the easy axis ( $\mathbf{M} \parallel [1\bar{1}0]$ ), the orbital moment of the Fe surface layer is very small, and in general couples antiparallel to its spin moment. For the cases with 1–2 W substrate layers, the orbital moment in the first substrate layer couples antiparallel to its spin moment (and parallel to the spin moment of Fe). However, already with the addition of the the third substrate layer, the orbital moment of the first substrate layer couples in parallel to its spin moment (and antiparallel to the Fe spin moment). For magnetization along the hard axis ( $\mathbf{M} \parallel [001]$ ) and perpendicular to the surface plane ( $\mathbf{M} \parallel [110]$ ), the coupling picture is opposite. The orbital moment of the Fe atom is still very small, but now coupled in parallel to its spin moment, and the orbital moment of the first W substrate layer couples in parallel to its spin moment for the cases with 1–2 W substrate layers (and antiparallel to the spin moment of the Fe surface layer). The rather large orbital moments of  $W_1$  for  $N_W = 1$  and 2 might occur due to the fact that these systems tend to have molecular properties rather than solid-state ones. They might originate in a combination of the large spin-orbit coupling found in W in combination with the large Fe moment. From the addition of the third substrate layer and onwards, the orbital moments of the first W atom couple antiparallel to their spin moments (and parallel to the Fe spin moment). Thus, with respect to the orbital moments, we conclude (i) that three substrate layers already deliver a converged result, and (ii) that in agreement with the observations made by Refs 13,42, Hund’s 3rd rule is broken for the W substrate.

For the perpendicular magnetization direction ( $\mathbf{M} \parallel [110]$ ), our results for  $\mu_L$  differs qualitatively from those obtained in Ref. 13. In order to explain this difference, a number of calculations were performed on the symmetric slab, based on the hypotheses that the difference is caused by (i) instabilities in the computer code, (ii) the perturbative final addition of the spin-orbit coupling in Ref. 13, (iii) the amount of “vac-

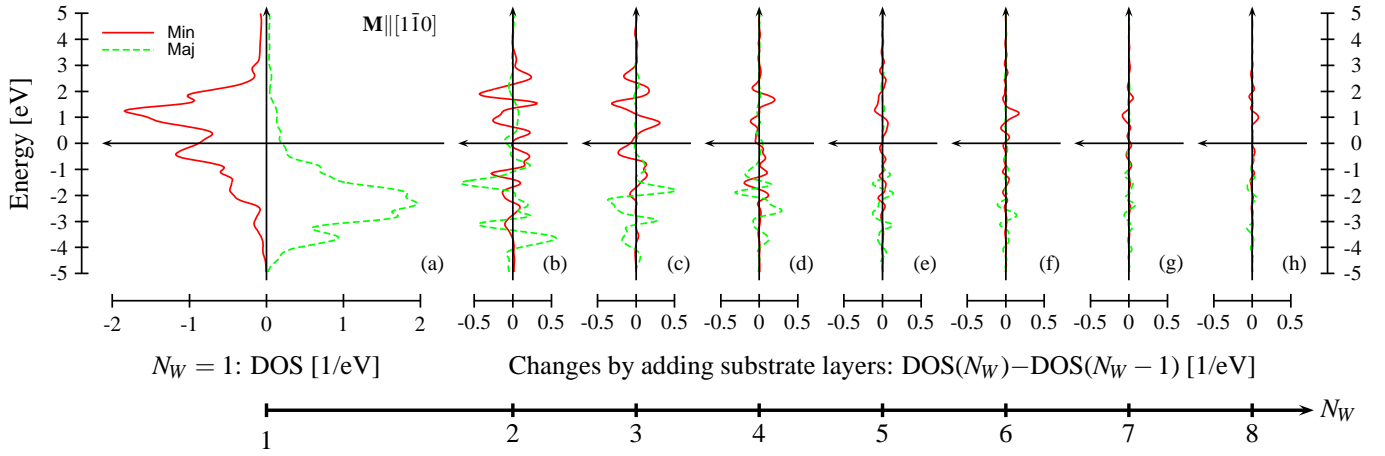


FIG. 2: (Color online) Evolution in the density of d-states (d-DOS) for an Fe(110) monolayer magnetized along the easy axis ( $\mathbf{M}||[1\bar{1}0]$ ) when up to 8 W(110) substrate layers are grown underneath it. The plot to the left (a) shows the density of states for the d-electrons of the Fe atom for an Fe monolayer with a single W substrate layer underneath. The d-DOS for the minority spin has been plotted with reverse sign for ease of understanding. The plots (b)–(h) shows the *changes* in the d-DOS of the Fe surface layer when additional W substrate layers are added underneath. In order to guide the eye, the scales are kept in constant proportion in all plots. On the energy scales, the Fermi energy is taken as the reference point ( $E_F = 0$ ). In all plots, red (full) lines are the results for the minority spin channel and green (dashed) lines are the results for the majority spin channel. In order to assure a good view of the plots we have moved the scales to the border of the figure.

TABLE III: Magnetic spin ( $\mu_S$ ) and orbital ( $\mu_L$ ) moments per atom (in Bohr magnetons,  $\mu_B$ ) are shown for the pseudomorphic Fe surface layer as well as the first W substrate layer ( $W_1$ ) as a function of the number of substrate layers ( $N_W$ ) when the magnetization is along the in-plane easy axis (columns 2–5), the in-plane hard axis (columns 6–9), and perpendicular to the surface (columns 10–13).

$N_W$	Easy axis: $\mathbf{M}  [1\bar{1}0]$				Hard axis: $\mathbf{M}  [001]$				Perpendicular: $\mathbf{M}  [110]$			
	Surface: Fe		Substrate: $W_1$		Surface: Fe		Substrate: $W_1$		Surface: Fe		Substrate: $W_1$	
	$\mu_S$	$\mu_L$	$\mu_S$	$\mu_L$	$\mu_S$	$\mu_L$	$\mu_S$	$\mu_L$	$\mu_S$	$\mu_L$	$\mu_S$	$\mu_L$
1	2.562	-0.00023	-0.135	5.792	2.561	0.00005	-0.136	-2.184	2.560	0.00007	-0.135	-0.584
2	2.574	-0.00010	-0.100	2.517	2.574	0.00009	-0.099	-3.449	2.570	0.00007	-0.102	-1.359
3	2.616	-0.00006	-0.089	-0.021	2.613	0.00005	-0.091	0.021	2.609	0.00005	-0.094	0.024
4	2.561	-0.00006	-0.104	-0.025	2.557	0.00005	-0.105	0.024	2.559	0.00005	-0.104	0.028
5	2.567	-0.00006	-0.098	-0.024	2.563	0.00004	-0.100	0.023	2.565	0.00005	-0.099	0.026
6	2.568	-0.00005	-0.101	-0.024	2.567	0.00004	-0.101	0.023	2.567	0.00005	-0.100	0.027
7	2.559	-0.00005	-0.104	-0.025	2.558	0.00004	-0.104	0.024	2.558	0.00005	-0.104	0.028
8	2.565	-0.00005	-0.103	-0.025	2.563	0.00004	-0.103	0.024	2.562	0.00005	-0.103	0.028

uum” between the slabs in the supercell calculation, or (iv) the breaking of the symmetry in the slab (removing one of the Fe surfaces). A repetition of the calculation in Ref. 13 eliminates the first hypothesis. A comparison between the repeated calculation and one with spin-orbit coupling included self-consistently leads to elimination of the second hypothesis.<sup>40</sup> In the symmetric slab, the Fe layers may couple electronically to each other either through the W substrate or through the vacuum. In Ref. 13, the distance through the W substrate is 24.52 Bohr, and the distance through the vacuum is 26.01 Bohr. Thus, in order to test hypothesis (iii) against hypothesis (iv) we increase the distance between the two Fe layers on the vacuum side to 76.54 Bohr.<sup>41</sup> The result of the calculation with the increased spacing on the vacuum side between the two Fe surfaces is [in support of hypothesis (iii)] an orbital moment for the Fe layer of  $0.00005\mu_B$  and an orbital moment for the first W layer of  $0.028\mu_B$ , in agreement with Tab. III. Thus, in agreement with Refs 42,43, we may conclude from

this little exercise on the symmetric slabs and from Tab. III that both the size as well as the alignment of the orbital moments in the Fe surface layer and the first W substrate layer are not only very sensitive to the local structure, but also to the direction of magnetization in the Fe layer.

In order to determine the influence of the substrate layers on the electronic properties of the magnetic surface, the evolution in the density of states for the d-electrons (d-DOS) of the Fe atom has been plotted in Fig. 2 (easy-axis magnetization,  $\mathbf{M}||[1\bar{1}0]$ ), beginning with the Fe/W(110) bilayer result in Fig. 2(a). In Figs. 2(b)–(h), the differences due to the addition of a second, third, fourth, fifth, sixth, seventh, and eighth substrate layer, respectively, are depicted on the same scale as the d-DOS of the bilayer. It is clear from Fig. 2 that the main features of the d-DOS of the Fe(110) surface layer are to be found in a band between 4 eV above and 5 eV below the Fermi energy ( $E_F = 0$  in Fig. 2). Also, we observe from Fig. 2 that by adding substrate layers, the changes to the d-DOS of the Fe

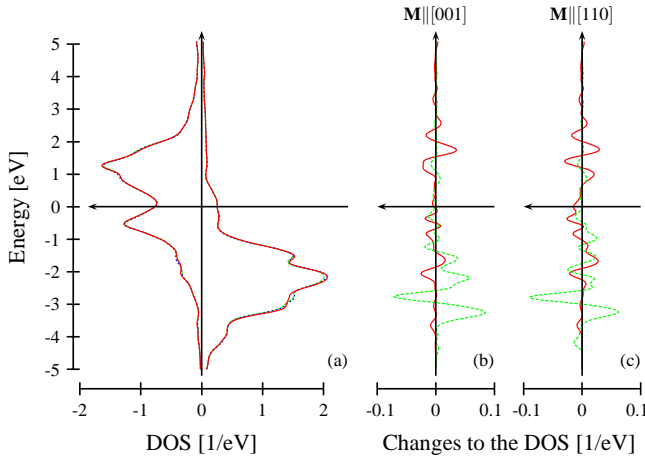


FIG. 3: (Color online) The density of d-electrons of the Fe atom (d-DOS) is shown for the calculation that has converged with respect to the number of substrate layers, i.e., for  $N_W = 4$ . Results are shown in the combined plot (a) for the easy (red, full line), hard [green, long-dashed line), and perpendicular (blue, short-dashed line) directions of magnetization, and (b)–(c) show the differences in the Fe d-DOS between (b) the easy and hard axes and between (c) the easy and perpendicular axes, respectively. In (b) and (c), the differences in the minority spin channel are plotted in red (full lines), and the differences in the majority spin channel in green (dashed lines). For ease of understanding, the d-DOS of the minority spin has been plotted with reverse sign, as in Fig. 2. Again, the zero on the energy scale corresponds to the Fermi energy and, again, we have put the scales to the border of the figure.

surface layer become less and less pronounced, as the number of substrate layers go up. Since already after the fourth or fifth substrate layer, the d-DOS of the Fe surface layer has converged to within a few percent of what it would be on bulk W(110), the d-DOS supports the conclusion that the MAEs have reached their bulk value after adding 4–5 substrate layers.

When the d-DOS has converged, the differences in d-DOS due to changes in the magnetization direction are very subtle. In order to illustrate this, we have in Fig. 3(a) plotted the d-DOS of an Fe(110) monolayer with four W substrate layers underneath it for the three cases where the magnetization direction is along one of the three main crystallographic axes. From Fig. 3(a) we notice that the d-DOS is now almost identical in all three cases. In order to explore the sub-

tle differences in the d-DOS between the different magnetization directions, we have in Figs. 3(b)–(c) additionally plotted the differences in the d-DOS between the easy axis, the hard axis, and the axis perpendicular to the surface, i.e., the two quantities  $\text{d-DOS}(\mathbf{M}||[\bar{1}\bar{1}0]) - \text{d-DOS}(\mathbf{M}||[001])$ , and  $\text{d-DOS}(\mathbf{M}||[\bar{1}\bar{1}0]) - \text{d-DOS}(\mathbf{M}||[110])$ , respectively. In contrast to the evolution of the d-DOS when adding substrate layers, the differences in the d-DOS between the different magnetization directions are too small to be plotted on the same scale as the d-DOS itself. Since the MAEs are in the meV-range, this is to be expected, since large changes in the d-DOS would lead to large MAEs.

#### IV. CONCLUSIONS

We have shown that the magnetocrystalline anisotropy energy in an Fe(110) monolayer on W(110) can be converged with respect to the thickness of the substrate using *ab initio* methods. After showing large changes for the first few substrate layers, it stabilized close to 3 meV, close to the experimental value. In addition, the directions of the easy and hard axes came out consistently, and in-plane. As expected from the large variations in the MAEs with respect to the addition of the first few substrate layers, also the density of the Fe d-states vary a lot during the addition of the first few substrate layers, after which it stabilizes. At the bulk-like substrate thicknesses, the differences between the density of d-states between the different magnetization directions reflects the fact that the MAE is in the meV regime (they are very small).

#### Acknowledgements

We acknowledge financial support from (i) the European Union FP5 Research Training Networks “First-Principles Approach to the Calculation of Optical Properties of Solids” (EXCITING) and “Dynamics in Magnetic Nanostructures” (Dynamics), under Contracts No. HPRN-CT-2002-00317 and HPRN-CT-2002-00289, respectively, (ii) Deutsche Forschungsgemeinschaft SPP 1133 “Ultraschnelle Magnetisierungsprozesse” and SPP 1153 “Cluster in Kontakt mit Oberflächen”, and (iii) Forschungsschwerpunkt des Landes Rheinland-Pfalz “Materialien für Mikro- und Nanosysteme” (MINAS).

- <sup>1</sup> H. J. Elmers, J. Hauschild, H. Höche, U. Gradmann, H. Bethge, D. Heuer, and U. Köhler, *Phys. Rev. Lett.* **73**, 898 (1994).
- <sup>2</sup> R. Röhlberger, J. Bansmann, V. Senz, K. L. Jonas, A. Bettac, U. Leopold, R. Rüffer, E. Burkel, and K. H. Meiwes-Broer, *Phys. Rev. Lett.* **86**, 5597 (2001).
- <sup>3</sup> U. Gradmann, M. Przybylski, H. J. Elmers, and G. Liu, *Appl. Phys. A* **49**, 563 (1989).
- <sup>4</sup> H. J. Elmers and U. Gradmann, *Appl. Phys. A* **51**, 255 (1990).
- <sup>5</sup> H. J. Elmers, T. Furubayashi, M. Albrecht, and U. Gradmann, *J. Appl. Phys.* **70**, 5764 (1991).

- <sup>6</sup> H. J. Elmers, J. Hauschild, H. Fritzsche, G. Liu, U. Gradmann, and U. Köhler, *Phys. Rev. Lett.* **75**, 2031 (1995).
- <sup>7</sup> M. Bode, O. Pietzsch, A. Kubetzka, and R. Wiesendanger, *Phys. Rev. Lett.* **92**, 067201 (2004).
- <sup>8</sup> S. Krause, L. Berbil-Bautista, M. Bode, and R. Wiesendanger, *Verhandl. DPG (VI)* **41**, 1/MA27.10 (2006).
- <sup>9</sup> U. Gradmann, J. Korecki, and G. Waller, *Appl. Phys. A* **39**, 101 (1986).
- <sup>10</sup> H. J. Elmers, J. Hauschild, and U. Gradmann, *Phys. Rev. B* **59**, 3688 (1999).

- <sup>11</sup> D. Sander, R. Skomski, C. Schmidthals, A. Enders, and J. Kirschner, Phys. Rev. Lett. **77**, 2566 (1996).
- <sup>12</sup> N. Weber, K. Wagner, H. J. Elmers, J. Hauschild, and U. Gradmann, Phys. Rev. B **55**, 14121 (1997).
- <sup>13</sup> X. Qian and W. Hübner, Phys. Rev. B **64**, 092402 (2001).
- <sup>14</sup> M. Bode, R. Pascal, and R. Wiesendanger, J. Vac. Sci. Technol. A **15**, 1285 (1997).
- <sup>15</sup> G. Waller and U. Gradmann, Phys. Rev. B **26**, 6330 (1982).
- <sup>16</sup> B. Hillebrands, P. Baumgart, and G. Günterodt, Phys. Rev. B **36**, 2450 (1987).
- <sup>17</sup> F. Gerhardter, Y. Li, and K. Baberschke, Phys. Rev. B **47**, 11204 (1993).
- <sup>18</sup> I.-G. Baek, H. G. Lee, H.-J. Kim, and E. Vescovo, Phys. Rev. B **67**, 075401 (2003).
- <sup>19</sup> K. von Bergmann, M. Bode, and R. Wiesendanger, Phys. Rev. B **70**, 174455 (2004).
- <sup>20</sup> A. Kubetzka, P. Ferriani, M. Bode, S. Heinze, G. Bihlmayer, K. von Bergmann, O. Pietzsch, S. Blügel, and R. Wiesendanger, Phys. Rev. Lett. **94**, 087204 (2005).
- <sup>21</sup> D. Spišák and J. Hafner, Phys. Rev. B **70**, 195426 (2004).
- <sup>22</sup> P. Ferriani, S. Heinze, G. Bihlmayer, and S. Blügel, Phys. Rev. B **72**, 024452 (2005).
- <sup>23</sup> X. Qian and W. Hübner, Phys. Rev. B **60**, 16192 (1999).
- <sup>24</sup> X. Qian, F. Wagner, M. Petersen, and W. Hübner, J. Magn. Magn. Mater. **213**, 12 (2000).
- <sup>25</sup> I. Galanakis, M. Alouani, and H. Dreyssé, Phys. Rev. B **62**, 3923 (2000).
- <sup>26</sup> H. L. Meyerheim, D. Sander, R. Popescu, J. Kirschner, O. Robach, and S. Ferrer, Phys. Rev. Lett. **93**, 156105 (2004).
- <sup>27</sup> J. W. Strutt, Phil. Trans. Roy. Soc. **161**, 77 (1870).
- <sup>28</sup> W. Ritz, J. reine angew. Math. **135**, 1 (1908).
- <sup>29</sup> E. Sjöstedt, L. Nordström, and D. J. Singh, Solid State Commun. **114**, 15 (2000).
- <sup>30</sup> P. Blaha, K. Schwarz, G. K. H. Madsen, D. Kvasnicka, and J. Luitz, *WIEN2k, An Augmented Plane Wave + Local Orbitals Program for Calculating Crystal Properties* (Karlheinz Schwarz, Vienna, 2001), ISBN 3-9501031-1-2.
- <sup>31</sup> D. Sander, A. Enders, and J. Kirschner, J. Magn. Magn. Mater. **200**, 439 (1999).
- <sup>32</sup> J. P. Perdew, K. Burke, and M. Ernzerhof, Phys. Rev. Lett. **77**, 3865 (1996); *ibid* **78**, 1396(E) (1997).
- <sup>33</sup> It should be noted here, that in order to secure a sufficiently accurate *magnetic* ground state, the spin-orbit coupling should be included self-consistently in the variational minimization of the total energy. Previously,<sup>23</sup>, the *nonmagnetic* ground state was converged self-consistently, and the spin-orbit coupling was added perturbatively at the end of the calculation.
- <sup>34</sup> The core states were calculated with 781 radial mesh points.
- <sup>35</sup> M. Pratzner, H. J. Elmers, M. Bode, O. Pietzsch, A. Kubetzka, and R. Wiesendanger, Phys. Rev. Lett. **87**, 127201 (2001).
- <sup>36</sup> H. J. Elmers, G. Liu, and U. Gradmann, Phys. Rev. Lett. **63**, 566 (1989).
- <sup>37</sup> J. Hauschild, H. J. Elmers, and U. Gradmann, Phys. Rev. B **57**, 677 (1998).
- <sup>38</sup> With respect to the results of the symmetric Fe/W(110) structures of Ref. 13, it is interesting to notice that removing the Fe layer on one side of the W(110) slab influences the MAEs in a manner a bit similar to (although not as strong as) that of adding an extra Fe layer on both sides of the slab, i.e., we obtain an in-plane hard axis and a slightly smaller anisotropy energy.
- <sup>39</sup> X. Qian and W. Hübner, Phys. Rev. B **67**, 184414 (2003).
- <sup>40</sup> The results for the orbital moments in these two calculations are consistent to within 10% in magnitude with those in Ref. 39, and the signs are identical. In order to assure sufficient accuracy in these two calculations, we have used  $T_c = 9$  and  $\#k = 2883$  here.
- <sup>41</sup> Thereby making the height of the unit cell comparable to the one used in the present calculations. For this comparison calculation, we used  $T_c = 9$  and  $\#k = 1521$ .
- <sup>42</sup> F. Wilhelm, P. Pouloupoulos, H. Wende, A. Scherz, K. Baberschke, M. Angelakeris, N. K. Flevaris, and A. Rogalev, Phys. Rev. Lett. **87**, 207202 (2001); *ibid* **90**, 129702 (2003).
- <sup>43</sup> R. Tyer, G. van der Laan, W. M. Temmermann, and Z. Szotek, Phys. Rev. Lett. **90**, 129701 (2003).